# Charge-Ordered States and the Phase Diagram of the Extended Hubbard Model on the Bethe lattice

Aleksey Alekseev[*] and Konrad Jerzy Kapcia[†]

*Institute of Spintronics and Quantum Information, Faculty of Physics and Astronomy,*
*Adam Mickiewicz University in Poznań, Uniwersytetu Poznańskiego 2, PL-61614 Poznań, Poland*

(Dated: November 21, 2025)

We study the extended Hubbard model (EHM) with both onsite Hubbard interaction and the intersite density-density interaction between nearest-neighbors using the standard Hartree mean-field approximation (MFA) on the Bethe lattice. We found that, at the ground state, the system can be in a charge-ordered insulating (COI), a charge-order metallic (COM) or a non-charge-ordered (NO) state. Moreover, the finite-temperature phase diagrams are presented. Several observables like a charge-order parameter, a spectral function, and particularly at finite temperatures, a charge carrier concentration (to visualize the degree of metallicity) are analyzed. The results show that increasing onsite repulsion suppresses charge order and change the properties of the system from insulating to metallic. Worth noting, that a number of phenomena can be found within the MFA, where their analysis is much simpler than in more advanced approaches. The method used for the EHM on the Bethe lattice also allows for a series of analytical derivations and simplification to see general geometry-independent features and analytical results, avoiding the numerical inaccuracies and other issues that appear with a purely numerical solution.

Keywords: extended Hubbard model, Bethe lattice, charge order, metal-insulator transition, mean-field approximation, phase diagram

## I. INTRODUCTION

Charge-order phenomena have been widely observed in various real compounds and have attracted broad interest not least due to its interplay and competition with superconductivity [1–3]. For instance they have been evidenced experimentally in hole-doped perovskite-type transition-metal oxides (cuprates, manganites, bismutates), transition-metal dichalcogenides [4, 5], numerous organic compounds, [6, 7], moiré systems [8], heavy-fermion systems, and various systems with alternating (mixed) valence. These phenomena encompasses Wigner crystals, including their generalized version, charge-density waves, charge-transfer insulators [9–11].

The model for investigation of the charge ordering is the extended Hubbard model (EHM) [12–16], which is, despite its simplicity, the most natural improvement of even more simple and artificial Hubbard model [17–20] that provided a lot of valuable insights into strongly-correlated physics. In this paper we study the EHM with onsite and intersite (nearest-neighbor) density-density interactions without attachment to a particular class of materials. We consider such studies of a model itself an advantageous step towards understanding of possible charge-order phenomena and mechanisms of their formation, as well as hints where to look for unusual phenomena. Worth noting, we investigate the model in the grand canonical ensemble with an all-encompassing range of chemical potentials without limiting to a particular filling factors. To our knowledge, such an approach is often ignored despite the fact that the fixed-occupation approach can result in incorrect phase diagram when the chosen occupation appears within phase-separation states. The phase-separation states correspond to the case where two phases with discontinuous transition between each other macroscopically coexist to form the state with intermediate spatially-averaged order parameter that lies within the range of the discontinuous jump of this parameter.

The model has been investigated within the atomic limit (without hopping term) [21–29], including also the Monte Carlo method [30–32]. The investigation within the broken symmetry Hartree-Fock approximation with finite hopping amplitude can be found in [12, 13, 33] (particularly in the context of the high-temperature superconductors (cuprates) [1]). The spinless model corresponds to a model without the Hubbard (onsite interaction) term and has been investigated in [34–44]; the research so far concentrates on the case of half-filled band with nearest-neighbor hopping. There are dynamical mean-field theory (DMFT) studies for charge density $n = 1/2$ at zero temperature [45] and finite temperature [46]; for arbitrary charge density, onsite interaction $U = 2D$ and small intersite interaction $V = 1.2D, 1.4D$ ($D$ is a half-bandwidth) on the Bethe lattice [47]. The all-encompassing research within the DMFT for the same model can be found in Ref. [48]. Finally, there are the cellular DMFT results at $n = 1/2$ and zero temperature on a square lattice [49]; $GW$+DMFT results at $n = 1$ on a square lattice [50, 51]; and extended DMFT and $GW$+EDMFT results on square and cubic lattices for longer-range intersite interactions, $n = 1$ and close to it [52]. The results in other extension of DMFT have been also obtained [53–56].

---

[*] e-mail: aleksey.alekseev@amu.edu.pl; ORCID ID: https://orcid.org/0000-0001-5102-6647

[†] corresponding author; e-mail: konrad.kapcia@amu.edu.pl; ORCID ID: https://orcid.org/0000-0001-8842-1886

Here, we restrict ourselves to the case of commensurate checkerboard ordering on the alternate lattices and use the mean-field (broken-symmetry Hartree) approximation (MFA) with semicircular (Bethe) noninteracting density of states to solve the model. Despite existing ground-state results within DMFT for the same model [48], our research serves several purposes. First, our intention is to fill the gap in the literature to clearly track the correlation-induced effects when comparing it with the DMFT result. Worth noting, that a number of phenomena can be found within the MFA where their analysis is much simpler. We also consider finite temperatures in contrast to [48]. Second, the mean-field solution of the EHM on the Bethe lattice allows for a series of analytical derivations and simplifications. We consider it as a toy model to see general geometry-independent features and analytical results, while the paper itself can serve pedagogical purposes.

The work is organized as follows. In Sec. II, the model and the approach are introduced and the general expression are derived. Sec. III is devoted for important observables, which are useful for the phase identification. Sec. IV provides the results at the ground state (Sec. IV A for analytical expressions, whereas Sec. IV B for numerical results). In Sec. V the results for finite temperatures are presented. Finally, Sec. VI contains conclusions and final remarks.

## II. MODEL AND METHOD

In this work, we investigate the extended Hubbard model [1, 46, 48] in the form of

$$\hat{H} = -t \sum_{(i,j)\sigma} \hat{c}_{i\sigma}^\dagger \hat{c}_{j\sigma} + U \sum_i \hat{n}_{i\uparrow}\hat{n}_{i\downarrow} + \frac{V}{2} \sum_{(i,j)} \hat{n}_i\hat{n}_j - \mu\hat{N},$$
(1)

where $t$ is a hopping amplitude, $U$ and $V$ are density-density onsite and nearest-neighbor (NN) intersite interaction parameters, $\mu$ is a chemical potential, $\sum_{(i,j)}$ means a summation over all lattice sites $i$ and $j$ that are nearest neighbors to each other, $\sigma$ is a spin index ($\uparrow$, $\downarrow$), $\hat{c}_{i\sigma}^\dagger$ and $\hat{c}_{i\sigma}$ are creation and annihilation operators, $\hat{n}_{i\sigma} = \hat{c}_{i\sigma}^\dagger \hat{c}_{i\sigma}$ is an occupation number operator, $\hat{n}_i = \sum_\sigma \hat{n}_{i\sigma}$, and $\hat{N} = \sum_i \hat{n}_i$.

We consider the checkerboard ordering or equivalently a 2-sublattice assumption, where each NN pair consists of two lattice sites from different sublattices (sublattice index is $\alpha = A, B$). After the Fourier transform to a reciprocal space and a mean-field decoupling, neglecting exchange (Fock) and pairing (anomalous, superconducting) parts of the decoupling (i.e., $\hat{n}_{i\sigma}\hat{n}_{j\sigma'} \overset{\text{MF}}{=} n_{j\sigma'}\hat{n}_{i\sigma} + n_{i\sigma}\hat{n}_{j\sigma'} - n_{i\sigma}n_{j\sigma'}$, where $n_{i\sigma} \equiv \langle\hat{n}_{i\sigma}\rangle$), the

Hamiltonian (1) turns into a sum of independent terms:

$$\hat{H} = \sum_{\mathbf{k}\sigma} \left[ \varepsilon_{\mathbf{k}}\hat{c}_{A\mathbf{k}\sigma}^\dagger \hat{c}_{B\mathbf{k}\sigma} + \varepsilon_{\mathbf{k}}^*\hat{c}_{B\mathbf{k}\sigma}^\dagger \hat{c}_{A\mathbf{k}\sigma} \right.$$
$$\left. + E_{A\sigma}\hat{n}_{A\mathbf{k}\sigma} + E_{B\sigma}\hat{n}_{B\mathbf{k}\sigma} \right] + C.$$
(2)

It is also called the broken-symmetry Hartree-Fock approach, although without the Fock-part. Here, $\mathbf{k}$ is a reciprocal-space vector, $\varepsilon_{\mathbf{k}}$ are Fourier-transform components of the hopping term, $\sum_{\mathbf{k}}$ means a summation over $\frac{L}{2}$ vectors in the (reduced) first Brillouin zone, $L$ is the number of lattice sites enclosed by the periodic boundary conditions,

$$C = -\frac{L}{2}\left[ Un_{A\uparrow}n_{A\downarrow} + Un_{B\uparrow}n_{B\downarrow} + zVn_An_B \right] \quad (3)$$

is the constant term,

$$E_{\alpha\sigma} = Un_{\alpha\bar{\sigma}} + zVn_{\bar{\alpha}} - \mu, \quad (4)$$

$n_{\alpha\sigma} = \frac{2}{L}\sum_{i\in\alpha}n_{i\sigma} = \frac{2}{L}\sum_{\mathbf{k}}n_{\alpha\mathbf{k}\sigma}$, $n_\alpha = \sum_\sigma n_{\alpha\sigma}$, $z$ is the coordination number, and $\bar{\sigma}$ or $\bar{\alpha}$ denotes a spin or sublattice index, different from $\sigma$ or $\alpha$, respectively,

In this research, in correspondence to previous works, we focus on the charge-ordering phenomenon neglecting possible magnetic ordering. Thus, we take $n_{\alpha\sigma} = \frac{n_\alpha}{2}$, and hence $E_{\alpha\uparrow} = E_{\alpha\downarrow} \equiv E_\alpha$.

We use the total electron density ($n$) and charge polarization (charge-order parameter, $\Delta$) as the order parameters, defined as

$$n = \frac{1}{2}\left(n_A + n_B\right), \qquad \Delta = \frac{1}{2}\left(n_A - n_B\right). \quad (5)$$

Let us introduce the quantities

$$E_0 = \frac{E_A + E_B}{2} = \left(zV + \frac{U}{2}\right)n - \mu,$$
$$E_{AB} = \frac{E_B - E_A}{2} = \left(zV - \frac{U}{2}\right)\Delta, \quad (6)$$

which are useful in the following discussion, and their physical meaning is discussed in Sec. III. An analytical diagonalization of the Hamiltonian (2) gives the following self-consistent system of equations for the order parameters:

$$\begin{cases} n = & \frac{2}{L}\sum_{\mathbf{k}}[f_{\text{FD}}(\epsilon_{\mathbf{k}}^-) + f_{\text{FD}}(\epsilon_{\mathbf{k}}^+)], \\ \Delta = & \frac{2}{L}\sum_{\mathbf{k}}\frac{E_{AB}}{Q_{\mathbf{k}}}[f_{\text{FD}}(\epsilon_{\mathbf{k}}^-) - f_{\text{FD}}(\epsilon_{\mathbf{k}}^+)], \end{cases} \quad (7)$$

where

$$f_{\text{FD}}(\epsilon) = \frac{1}{1 + e^{\beta\epsilon}}, \quad (8)$$

is the Fermi-Dirac distribution, $\beta = T^{-1}$, $T$ is a temperature (for $\beta = \infty$, $f_{\text{FD}}(\epsilon) = \theta(-\epsilon)$, where $\theta$ is the Heaviside step function),

$$\epsilon_{\mathbf{k}}^\pm = E_0 \pm Q_{\mathbf{k}}, \qquad Q_{\mathbf{k}} = \sqrt{E_{AB}^2 + |\varepsilon_{\mathbf{k}}|^2}. \quad (9)$$

To investigate the model (1) we use a semicircular density of state (DOS) which is the noninteracting DOS of the Bethe lattice with $z \to \infty$:

$$\rho(\varepsilon) = \frac{2}{L} \sum_{\mathbf{k}} \delta(\varepsilon - \varepsilon_{\mathbf{k}})$$
$$= \frac{2}{\pi D} \sqrt{1 - \left(\frac{\varepsilon}{D}\right)^2}, \quad \text{for } |\varepsilon| < D \tag{10}$$

(per spin), were $D = 2t$. Note, that it is not that different from some cubic-lattice DOSs [57]. The corresponding noninteracting half-bandwidth as well as a typical kinetic energy is $2\sqrt{\int_{-\infty}^{\infty} \varepsilon^2 \rho(\varepsilon) d\varepsilon} = D$. We express the quantities, such as $U$, $zV$, $\mu$, and $T$, in the units of $D$ (or equivalently, we set $D = 1$). We also use the expression

$$\frac{2}{L} \sum_{\mathbf{k}} f(\varepsilon_{\mathbf{k}}) = \int \rho(\varepsilon) f(\varepsilon) d\varepsilon \tag{11}$$

to solve the self-consistent system (7). A strict convergence criterion of $10^{-12}$ is set for the order parameters.

To find which phase is stable in the coexistence regions (for fixed $\mu$) we compare their grand potentials expressed by

$$\Omega = C - \frac{2}{\beta} \sum_{\mathbf{k}} \ln \mathscr{Z}_{\mathbf{k}}, \tag{12}$$

where

$$\mathscr{Z}_{\mathbf{k}} = 1 + e^{-\beta \epsilon_{\mathbf{k}}^-} + e^{-\beta \epsilon_{\mathbf{k}}^+} + e^{-\beta(\epsilon_{\mathbf{k}}^- + \epsilon_{\mathbf{k}}^+)}. \tag{13}$$

For the ground state ($T = 0D$) it is also equal to the total energy ($E = \langle \hat{H} \rangle$) and takes a simplified form of

$$\Omega = E = C + 2 \sum_{\mathbf{k}} \min\{0, E_0 - Q_{\mathbf{k}}, 2E_0\}. \tag{14}$$

In the research, we make use of the shifted chemical potential defined as $\bar{\mu} = \mu - zV - \frac{U}{2}$, chosen that way that $\bar{\mu} = 0D$ corresponds to the half-filling of the lattice ($n = 1$) and it is also a point of a particle-hole symmetry (the results for $\bar{\mu} < 0D$ can be easily mapped to the $\bar{\mu} > 0D$).

The calculations for solving eqs. (7) are implemented in Python language, and the figures are made using its `matplotlib` library.

## III. SPECTRAL FUNCTION AND CHARGE CARRIERS

An additional tool to interpret the ground-state results is a spectral function ($A_{\alpha}(\omega + i\eta)$), while its value at the Fermi level ($\omega = 0D$) is another order parameter (the $\lim_{\eta \to +\infty} A_{\alpha}(i\eta)$ is zero for an insulating phase and nonzero for a metallic one). The spectral function ($\alpha$-sublattice projected) is calculated as

$$A_{\alpha}(\omega + i\eta) = -\frac{2}{\pi} \frac{2}{L} \sum_{\mathbf{k}} \text{Im} \, G_{\alpha\alpha\mathbf{k}\sigma}(\omega + i\eta) \tag{15}$$
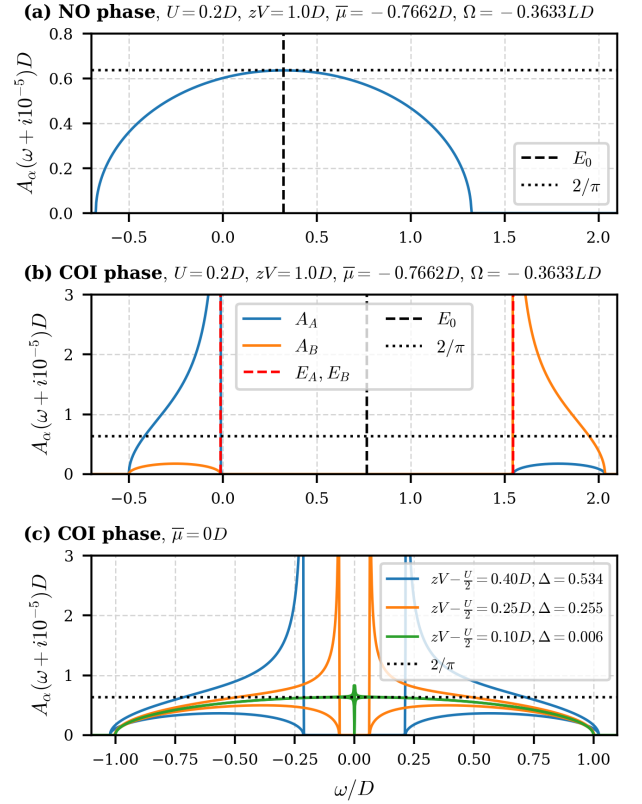


FIG. 1. Spectral functions for the ground state. (a) and (b) are spectral functions of the non-charge-ordered (NO, $n = 0.597$, $\Delta = 0$) metal and charge-ordered insulator (COI, $n = 1$, $\Delta = 0.865$) for the same point of the phase diagram where their grand potentials ($\Omega$) are equal (the point on a discontinuous phase transition line). (c) is a spectral function evolution of the COI phase at $\bar{\mu} = 0D$ when $zV - \frac{U}{2}$ approaches $0D$ (the continuous transition to the half-filled NO phase).

and the total spectral function is defined as

$$A(\omega + i\eta) = \sum_{\alpha} A_{\alpha}(\omega + i\eta), \tag{16}$$

with $\eta = 10^{-4}D$,

$$G_{\alpha\alpha\mathbf{k}\sigma}(z) = \frac{\xi_{\bar{\alpha}}(z)}{\xi_A(z)\xi_B(z) - |\varepsilon_{\mathbf{k}}|^2}, \tag{17}$$

and $\xi_{\alpha}(z) = z - E_{\alpha}$. With the semicircular noninteracting DOS (i.e., for the Bethe lattice) one gets:

$$\frac{2}{L} \sum_{\mathbf{k}} G_{\alpha\alpha\mathbf{k}\sigma} = \frac{2}{L} \sum_{\mathbf{k}} \frac{\xi_{\bar{\alpha}}}{\xi_A \xi_B - |\varepsilon_{\mathbf{k}}|^2}$$
$$= \begin{cases} \frac{\xi_{\bar{\alpha}}}{D^2}\left(1 - i\frac{\sqrt{D^2 - \xi_A \xi_B}}{\sqrt{\xi_A \xi_B}}\right), & \text{if } \text{Im}[\xi_A \xi_B] \geq 0, \\ \frac{\xi_{\bar{\alpha}}}{D^2}\left(1 + i\frac{\sqrt{D^2 - \xi_A \xi_B}}{\sqrt{\xi_A \xi_B}}\right), & \text{if } \text{Im}[\xi_A \xi_B] < 0. \end{cases} \tag{18}$$

Figs. 1a and 1b show typical shapes of the spectral function at $T = 0D$ for a non-charge-ordered (NO) phase with $\Delta = 0$ and a charge-ordered (CO) phase with $|\Delta| > 0$, respectively. Both of them are calculated for the same point of a ground-state phase diagram, where these two phases have the same total energy (the point of a discontinuous phase transition). For the NO phase, the $E_0 = E_A = E_B$, $E_{AB} = 0D$, and the spectral function is simply a semicircular DOS shifted by the value of $E_0$. At $\omega = E_0$ the spectral function is maximal and equal to $2/\pi$ (per sublattice). Note, that the self-consistent solution of the system (7) for the NO phase always exists within the mean-field approximation. At $T = 0D$, for the $|\bar{\mu}| \geq zV + \frac{U}{2} + D$, the NO phase is a fully-unoccupied or fully-occupied band insulator.

The spectral function of the CO phase shows two bands: the lower one primarily comes from a more occupied sublattice, and the upper one – from a less occupied sublattice. In the large-$V$ limit, the $n_\alpha$ are equal to 2 and 0, and there is a full correspondence between a sublattice and a band. At the ground state, the position of the Fermi level inside or outside of a band defines if the phase is a charge-ordered insulator (COI) or a charge-ordered metal (COM), respectively. The COI phase is always half-filled (i.e., $n_{COI} = 1$).

If the hopping is suppressed (atomic limit), the CO phase consists of two atomic levels at the points $E_A$ and $E_B$ with a gap $2|E_{AB}| = |E_B - E_A|$ and a middle point $E_0$ between them. With the finite hopping, the levels becomes finite-width bands. Usefully, the points $E_A$ and $E_B$ correspond to singularities at the very edges of the bands, so that the value of $2|E_{AB}|$ is a band gap at the ground state. Note, that there are severe convergence problems in the self-consistent system (7) for the COM phase when the Fermi level is close to the singularities (for $E_\alpha \approx 0D$).

At finite temperatures ($T > 0D$), the order parameter $A_\alpha(i\eta)$ does not provide useful information due to the thermal excitations beyond the Fermi level. Instead, to visualize the degree of metallicity or charge carrier concentration, we use the following quantity defined as

$$c = \int_{-\infty}^{0} A(\omega + i\eta)f_{FD}(-\omega)d\omega + \int_{0}^{\infty} A(\omega + i\eta)f_{FD}(\omega)d\omega. \quad (19)$$

Its physical meaning is a total concentration of conduction electrons and holes when such a division of charge carriers is still applicable. Note, that this quantity is zero at $T = 0D$ even for metallic phases, but it grows fast as $T$ increases.

## IV. GROUND-STATE RESULTS

### A. Simplified Expressions at $T = 0$

A number of simplifications of the self-consistent equations (7) are possible for the $T = 0D$ (ground state) case. Below we present analytical formulas in this limit.

#### 1. NO Phase

For the NO phase, the order parameter $\Delta = 0$ and the self-consistent equations reduce to

$$n_{NO} = \frac{2}{\pi}\arccos\frac{E_0}{D} - E_0\rho(E_0) \quad (20)$$

with $E_0$ from eq. (6). The expression for the total energy is also simplified to

$$\frac{E_{NO}}{L} = \frac{C}{L} + n_{NO}E_0 - \frac{\pi^2 D^4}{6}\rho(E_0)^3, \quad (21)$$

i.e., it is analytical as far as $n_{NO}$ is found numerically from eq. (20).

#### 2. COI Phase

Let us introduce a function

$$\mathcal{E}_h(x|m) = -i\mathcal{E}(i\operatorname{arcsinh} x\,|\,m) \quad (22)$$

where $\mathcal{E}(\varphi|m)$ is an incomplete elliptic integral of the second kind. Note, that the function does not actually contains imaginary units: $-i\mathcal{E}(i\varphi|m) = \int_0^\varphi \sqrt{1 + m\sinh^2\theta}\,d\theta$. We also use notations: $\mathcal{F}(\varphi|m)$ for the incomplete elliptic integral of the first kind ($\mathcal{F}(\varphi|m) = \int_0^\varphi(1 - m\sin^2\theta)^{-1/2}d\theta$), and $\mathcal{K}(m) = \mathcal{F}(\frac{\pi}{2}|m)$ and $\mathcal{E}(m) = \mathcal{E}(\frac{\pi}{2}|m)$ for the complete elliptic integrals.

For $\Delta \neq 0$ and $|E_0| \leq |E_{AB}|$, the system is always at the half-filling (i.e., $n = 1$) and the charge polarization becomes

$$\Delta_{COI} = \frac{4|E_{AB}|}{\pi D}\mathcal{E}_h\left(\frac{D}{E_{AB}}\,\middle|\,-\left(\frac{E_{AB}}{D}\right)^2\right)$$
$$= \frac{4|E_{AB}|}{\pi D}\frac{E_{AB}}{D}\left[(q^{-1}+1)\mathcal{K}(-q^{-1}) - \mathcal{E}(-q^{-1})\right], \quad (23)$$

where $q = \left(\frac{E_{AB}}{D}\right)^2$. The opposite is also correct: for $n = 1$ and $\Delta \neq 0$, the $|E_0|$ (which is also equal to the $|\bar{\mu}|$) is always less or equal to the $|E_{AB}|$. Thus, the eq. (23) is a self-consistent equation for the $\Delta$ of a half-filled CO phase, more specifically, of the COI phase. It does not require to perform numerical integration and numerically much more stable than the original equation. Notably, $\Delta_{COI}$ does not depend on $\mu$, as well as points $E_A$, $E_B$,
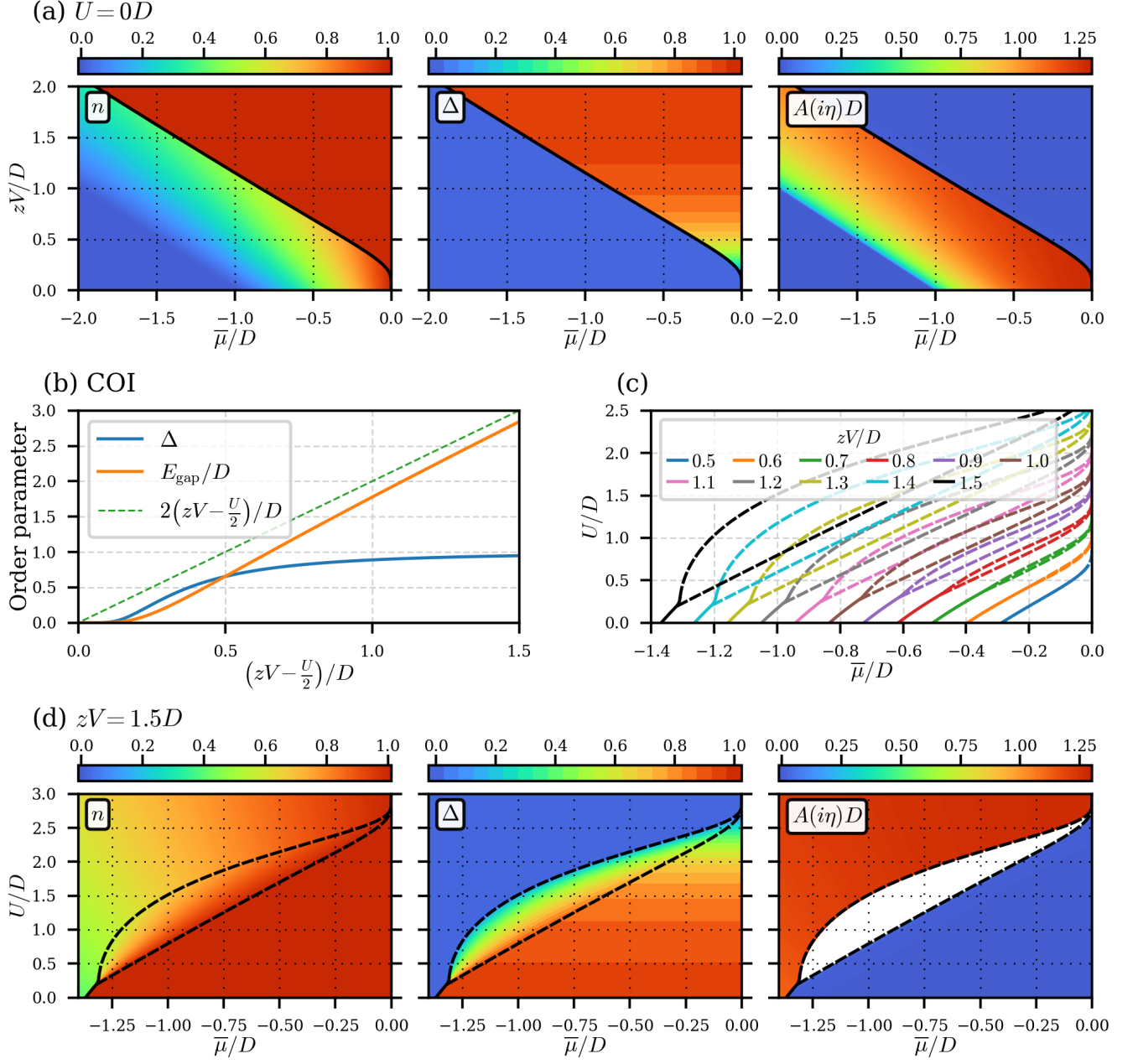
FIG. 2. Ground-state phase diagrams and properties. (a) $\bar{\mu}$-$V$ phase diagram for $U = 0D$; (b) dependencies of COI-phase properties; (c) evolution of the $\bar{\mu}$-$U$ phase diagram when $V$ changes; (d) $\bar{\mu}$-$U$ phase diagram for $V = 1.5D$. On the phase diagrams: dashed and solid black lines denote continuous and discontinuous transitions, respectively; color scales are for concentration $n$, charge polarization $\Delta$ and spectral function $A(i\eta)D$ (as labeled). The white region on the $A(i\eta)D$ color-contour plot corresponds to the model parameters, where the value of $A(i\eta)D$ is far out of a range of the presented colorbar (it is unrepresentative to extend the colorbar range), the corresponding phase is the COM phase. Only the phases with the lowest grand potential are shown (no metastable phases).

and the distance $E_{AB}$ on a spectral function plot. More-over, only the difference $(zV - \frac{U}{2})$ matters.

The condition $|E_{AB}| = |\bar{\mu}|$ defines points where the COI phase continuously changes into the COM phase (the point of a continuous transition, if the CO phases are stable with respect to the NO phase at this point). In the large $(zV - \frac{U}{2})$ limit, the $\Delta_{\text{COI}}$ asymptotically

approaches 1, and an asymptotic line of the continuous transition is determined as $(zV - \frac{U}{2}) = |\bar{\mu}|$.

A band gap of the COI phase is found as

$$E_{\text{gap}} = 2|E_{AB}| = 2\left(zV - \frac{U}{2}\right)|\Delta_{\text{COI}}|. \qquad (24)$$

Both quantities, $\Delta_{\text{COI}}$ and $E_{\text{gap}}$, are shown as a func-

tion of $(zV - U/2)/D$ in Fig. 2b.

The total energy of the COI phase is also simplified so that the numerical integration is not required. Note, that it helps to avoid numerical inaccuracies when the $zV - \frac{U}{2}$ is very small. The expression for the energy is

$$
\begin{aligned}
\frac{E_{\text{COI}}}{L} &= \frac{C}{L} - \bar{\mu} \\
&- \frac{4|E_{AB}|}{3\pi} \left[ (1+q)\mathcal{K}(-q^{-1}) + (1-q)\mathcal{E}(-q^{-1}) \right],
\end{aligned}
\tag{25}
$$

i.e., its only dependency on $\mu$ is the term $-\bar{\mu}$.

It is clear, that the second equation in the system (7) cannot yield $\Delta \neq 0$ (a CO phase) for $zV < \frac{U}{2}$. In fact, at $\bar{\mu} = 0D$ there is a continuous transition from the half-filled COI phase to the half-filled NO phase (COI-NO transition) exactly at $zV = \frac{U}{2}$. As $(zV - \frac{U}{2})$ approaches zero, from above, one gets

$$
\Delta_{\text{COI}} \approx \pm \frac{4D}{zV - \frac{U}{2}} \exp\left[ -\frac{\pi D}{4\left(zV - \frac{U}{2}\right)} - 1 \right].
\tag{26}
$$

The corresponding spectral functions of the COI phase are shown in Fig. 1c. The asymptotic behaviour of the $\Delta$ and the $(E_{\text{COI}} - E_{\text{NO}})$ around this continuous transition makes the COI and NO phases indistinguishable up to a machine precision ($\sim 10^{-16}$ for $(E_{\text{COI}} - E_{\text{NO}})/(LD)$) for a noticeable region of parameters ($zV - \frac{U}{2} \lesssim 0.05D$, see also Fig. 2b), while the original equations, that involve numerical integration, yield incorrect results for a larger region of $(zV - \frac{U}{2})$ (around $0.1D$). For this reason, the correct results in this region can be obtained with the presented analytical simplifications only.

### 3. COM Phase

When $|E_0| > |E_{AB}|$ and $\Delta \neq 0$, the set of equations describes the COM phase. The system of self-consistency equations reduces to

$$
\begin{cases}
n_{\text{COM}} = 1 - \text{sign}(E_0)\left[1 - n_c\left(-\sqrt{E_0^2 - E_{AB}^2}\right)\right] \\
\quad = \begin{cases} n_c\left(-\sqrt{E_0^2 - E_{AB}^2}\right), & E_0 > 0D, \\ 2 - n_c\left(-\sqrt{E_0^2 - E_{AB}^2}\right), & E_0 < 0D, \end{cases} \\
\Delta = \Delta_{\text{COI}} - \frac{4|E_{AB}|}{\pi D}\mathcal{E}_h\left(\frac{\sqrt{E_0^2 - E_{AB}^2}}{E_{AB}} \middle| -\left(\frac{E_{AB}}{D}\right)^2\right),
\end{cases}
\tag{27}
$$

where we have introduced the following function

$$
n_c(\mu) = \frac{2}{\pi}\arccos\left(\frac{-\mu}{D}\right) + \mu\rho(\mu),
\tag{28}
$$

which is a cumulative charge density when the noninteracting semicircular DOS is integrated and $\rho(\varepsilon)$ is defined by (10). Particularly, eq. (20) can be written as $n_{\text{NO}} = n_c(-E_0) = 2 - n_c(E_0)$.

The total energy for the COM phase is also simplified to the expression

$$
\begin{aligned}
\frac{E_{\text{COM}}}{L} &= \frac{C}{L} + E_{\text{COI}} + \frac{2E_0}{3}\sqrt{E_0^2 - E_{AB}^2} \cdot \rho\left(\sqrt{E_0^2 - E_{AB}^2}\right) \\
&+ \frac{4|E_{AB}|}{3\pi}\left[ (1+q)\mathcal{F}\left(\arcsin\frac{\sqrt{E_0^2 - E_{AB}^2}}{D} \middle| -q^{-1}\right) \right. \\
&\left. + (1-q)\mathcal{E}\left(\arcsin\frac{\sqrt{E_0^2 - E_{AB}^2}}{D} \middle| -q^{-1}\right) \right],
\end{aligned}
\tag{29}
$$

so that it does not require numerical integration as far as $n_{\text{COM}}$ and $\Delta$ are found.

The continuous transition COM-NO (when it exists) for specific $zV/D$ and $U/D$, can be easily located solving the following system of equations

$$
\begin{cases}
n = n_c(-E_0), \\
1 = \frac{4}{\pi D}\left(zV - \frac{U}{2}\right)\left(\log\left[1 + \frac{1}{D}\sqrt{D^2 - E_0^2}\right] \right. \\
\quad \left. - \log\frac{|E_0|}{D} - \frac{1}{D}\sqrt{D^2 - E_0^2}\right).
\end{cases}
\tag{30}
$$

with respect to $n$ and $\bar{\mu}$. The direct solution of the system (7) or simplified system (27) at the point of the continuous COM-NO transition requires extremely large (millions) number of iterations during which $\Delta$ slowly converges to 0. This makes using the system (30) advantageous. Moreover, usefully, when this system gives a solution at which $\Delta \neq 0$, it indicates, that the continuous transition COM-NO does not exist, and the transition is discontinuous only (at some other point).

### B. Results at $T = 0$

Fig. 2a shows the $U = 0D$ ground-state phase diagram at hole doping for a range of repulsive intersite interactions. Hereinafter, only the phases with the lowest grand potential $\Omega$ are shown on phase diagrams. The COI phase is identified as a phase with nonzero charge polarization ($\Delta \neq 0$), half-filling ($n = 1$), and the lack of the spectral weight at the Fermi level ($A(i\eta)D = 0$). As the chemical potential decreases, the COI phase discontinuously transitions to the NO metallic phase slightly before it would continuously transition to the COM phase (i.e., before $\bar{\mu}$ riches value $-\left(zV - \frac{U}{2}\right)|\Delta|$). At $\bar{\mu} = 0D$ the transition to the half-filled NO phase is continuous as follows from Fig. 2b. As mentioned before, the NO phase becomes a fully-unoccupied insulator for the $\bar{\mu} \leq -(zV + \frac{U}{2} + D)$.

When the onsite repulsion is nonzero and the chemical potential decreases, the COI phase can continuously transition to the COM phase ($0 < \Delta < 1$, $n_{\text{NO}} < n < 1$, $A(i\eta)D > 0$) before it gets unstable toward the NO phase (the example for $zV = 1.5D$ is shown in Fig. 2d). Thus, there is a point where the COI, NO, and COM phases meet, a ternary point ($V_{\text{tern}}, U_{\text{tern}}, \bar{\mu}_{\text{tern}}$). For
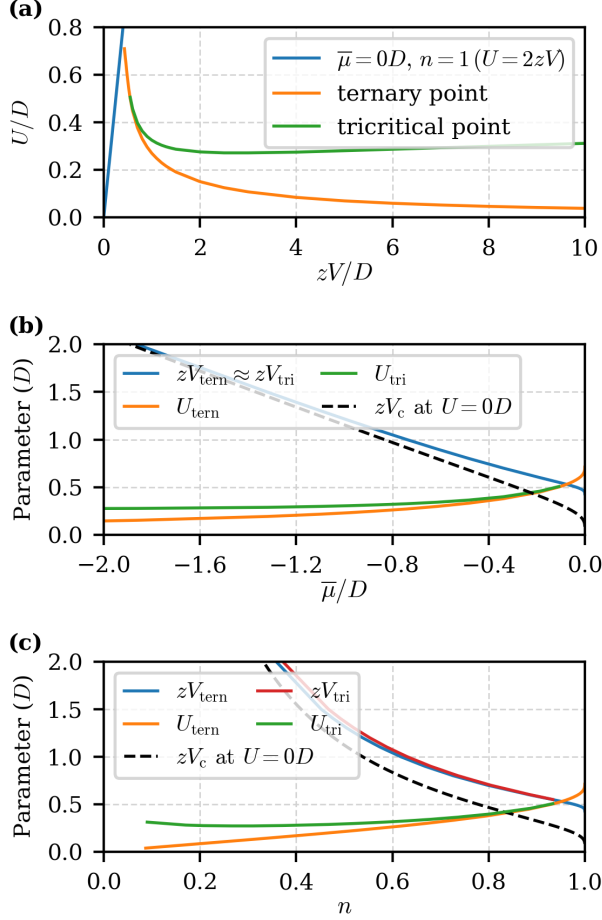
FIG. 3. Tendencies of the ground-state critical points: a relation between the interaction strengths of the critical points, alongside with a point of the continuous COI-NO transition at $\bar{\mu} = 0D$ (a); and dependencies of the interaction strengths of the critical points on the shifted chemical potential (b) and the electron density of the NO phase (c), alongside with a point of the discontinuous COI-NO transition at $U = 0D$ ($V_c$, Fig. 2a).

$U$ slightly larger than $U_{\text{tern}}$, the COM-NO transition is discontinuous similarly to the located nearby COI-NO transition. Further, however, the transition becomes continuous ($\Delta \to 0$, $n_{\text{COM}} \to n_{\text{NO}}$), and thus, a tricritical point ($V_{\text{tri}}$, $U_{\text{tri}}$, $\bar{\mu}_{\text{tri}}$) is identified. One can see the evolution of the $\bar{\mu}$-$U$ phase diagram for varying $V$ in Fig. 2c. Additionally, Fig. 3 shows the evolution of the ternary and tricritical points from different perspectives. The horizontal axis in Fig. 3c is the electron density of the NO phase ($n_{\text{NO}}$), because at the ternary point the $n_{\text{COI}}$ and $n_{\text{COM}}$ always equal 1, and at the tricritical point $n_{\text{COM}} = n_{\text{NO}}$. For a fixed $V$, $\bar{\mu}_{\text{tern}} \approx \bar{\mu}_{\text{tri}}$, and vice versa, for a fixed $\bar{\mu}$, $V_{\text{tern}} \approx V_{\text{tri}}$.

Since the electron density experiences a jump at the point of discontinuous transition, a range of $n$ can manifest itself within the macroscopic phase separation only.

It can be found with the Maxwell's construction as, e.g., in [26, 58, 59]. The range of repulsive interaction parameters where the phase separation takes place is everything below the line of tricritical points in Fig. 3a. As the intersite interaction increases, the ternary point asymptotically approaches the $U = 0D$, while the $U_{\text{tri}}$ slightly increases, hence the range of $U$ with the phase separation increases as well.

For small intersite interaction, ternary and tricritical points approach the point of the continuous COI-NO transition at $\bar{\mu} = 0D$. A special critical point of the ground-state phase diagram is when the ternary point, the tricritical point, and the point of transition at the half-filling merge together (see Fig. 3a): $zV \approx 0.4D$ ($U = 2zV$, $\bar{\mu} = 0D$, $n = 1$). Although we cannot distinguish the tricritical point from the ternary point even earlier due to their asymptotic approach to each other, it is clear that they can merge at $\bar{\mu} = 0D$ only, because the COI phase ($n_{\text{COI}} = 1$) cannot continuously transition to the NO phase at $\bar{\mu} \neq 0D$ ($n \neq 1$). Thus, for $zV \lesssim 0.4D$ the COM phase does not exist and the symmetry-breaking transition is always discontinuous except for the transition at $\bar{\mu} = 0D$.

## V. FINITE-TEMPERATURE RESULTS

Finite temperatures destroy the charge order i.e., in large enough temperatures, only the NO phase occurs. The character of this transition depends on the part of the phase diagram.

### A. Simplified Expressions at $T > 0$

For the $\bar{\mu} = 0D$, there is one-to-one correspondence between the difference ($zV - \frac{U}{2}$) and a critical temperature $T_c$ of the continuous CO-NO transition (cf. also Refs. [12, 13]):

$$zV - \frac{U}{2} = \left( \frac{2}{\pi D^2} \int_{-D}^{D} d\varepsilon \frac{\sqrt{D^2 - \varepsilon^2}}{\varepsilon} \tanh\left[ \frac{\varepsilon}{2T_c} \right] \right)^{-1}.$$
(31)

It is shown in Fig. 4a, and is also the highest temperature at which CO can exist (see phase diagrams in Fig. 4b). It has an asymptotic behaviour in the large ($zV - \frac{U}{2}$) limit:

$$T_c \approx \frac{1}{2}\left( zV - \frac{U}{2} \right).$$
(32)

For an arbitrary filling, the self-consistency equations for the continuous CO-NO transition (when it exists) are not simplified much, but it is still useful to find it solving

$$\begin{cases} n = \int d\varepsilon \rho(\varepsilon) \left[ f_{\text{FD}}(\frac{E_0 - \varepsilon}{T_c}) + f_{\text{FD}}(\frac{E_0 + \varepsilon}{T_c}) \right], \\ 1 = \left( zV - \frac{U}{2} \right) \int d\varepsilon \frac{\rho(\varepsilon)}{\varepsilon} \left[ f_{\text{FD}}(\frac{E_0 - \varepsilon}{T_c}) - f_{\text{FD}}(\frac{E_0 + \varepsilon}{T_c}) \right], \end{cases}$$
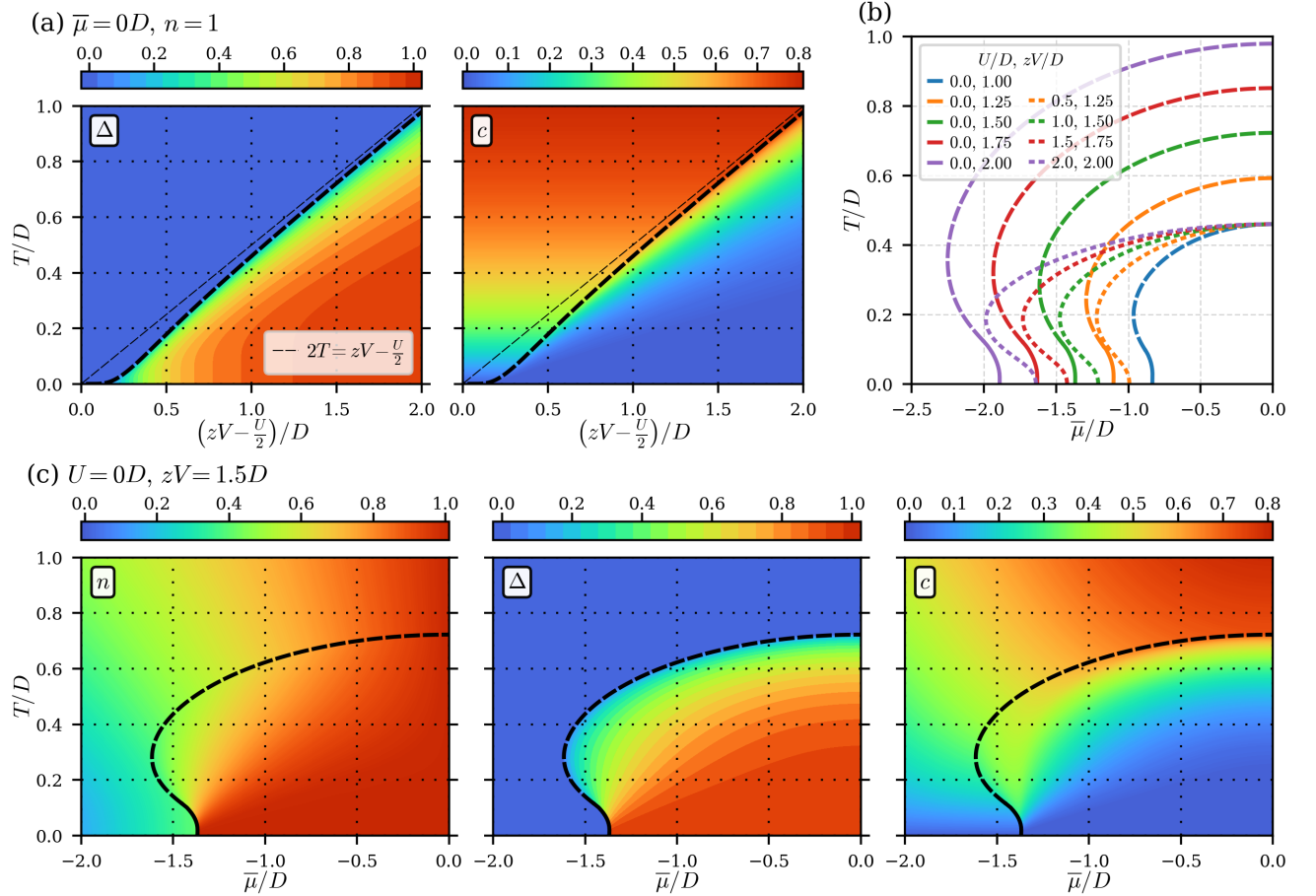(33)

FIG. 4. Finite-temperature phase diagrams. (a) the $(zV - \frac{U}{2})$-$T$ phase diagram for $\bar{\mu} = 0D$; (b) the evolution of the $\bar{\mu}$-$T$ phase diagram when the interaction strengths change; (c) the $\bar{\mu}$-$T$ phase diagram for $U = 0D$ and $V = 1.5D$. On the phase diagrams: dashed and solid black lines are for continuous and discontinuous transitions, respectively; color scales are for concentration $n$, charge polarization $\Delta$ and charge carrier concentration $c$ (as labeled). Both short and long dashed lines on panel (b) denote continuous transitions and are different to distinguish the $U = 0D$ lines and the $zV - \frac{U}{2} = 1D$ lines. Only the phases with the lowest grand potential are shown (no metastable phases).

instead of straightforward solution of the model on a grid of parameters. Moreover, the same notes as previously mentioned for the system of equations (30) are valid: the convergence at the continuous transition point is extremely slow, and the solution with $\Delta \neq 0$ indicates the discontinuous character of the transition.

## B. Results at $T > 0$

An example of the $U = 0D$ finite-temperature phase diagram is shown in Fig. 4c. It is similar to those presented in Refs. [35, 42, 43, 60] for the spinless fermion model. At finite temperatures there is no clear distinction between the COI and COM phases. At low temperatures, the CO-NO transition stays discontinuous, and thus there is a range of electron density that is possible within the phase separation states only. On the scale of the shown plot the metastability region of the CO phase

inside the NO phase is not significant – around $0.04D$ for $T = 0D$ and smaller for larger $T$.

With the increase of temperature the transition becomes continuous, thus, a tricritical point is identified $(T_{\mathrm{tri}}, V_{\mathrm{tri}}, \bar{\mu}_{\mathrm{tri}})$. Solid and long dashed lined in Fig. 4b show the evolution of $U = 0D$ phase diagrams as the intersite interaction $V$ varies. As it was clear from the combination of the $T = 0D$ phase diagram (Fig. 2a) and the $\bar{\mu} = 0D$ phase diagram (Fig. 4a), the parameter range of ordered phases proportionally increases when $V$ increases. The coordinates of the tricritical point from the different perspective and for $U = 0D$ are shown in Fig. 5. The $zV$- and $T$-parameter ranges when the phase separation takes place is below the line of tricritical points in Fig. 5a; the temperature in this region should not exceed $0.15D$ unless one deals with unreasonable values of $zV$ (where the mean-field approximation likely fails). We present data for the tricritical point for $U = 0D$ only. It is not relevant for $U \gtrsim 0.3 - 0.5D$ at which there is no discontinuous transition already for $T = 0D$ (Fig. 3a).

$U = 0D$
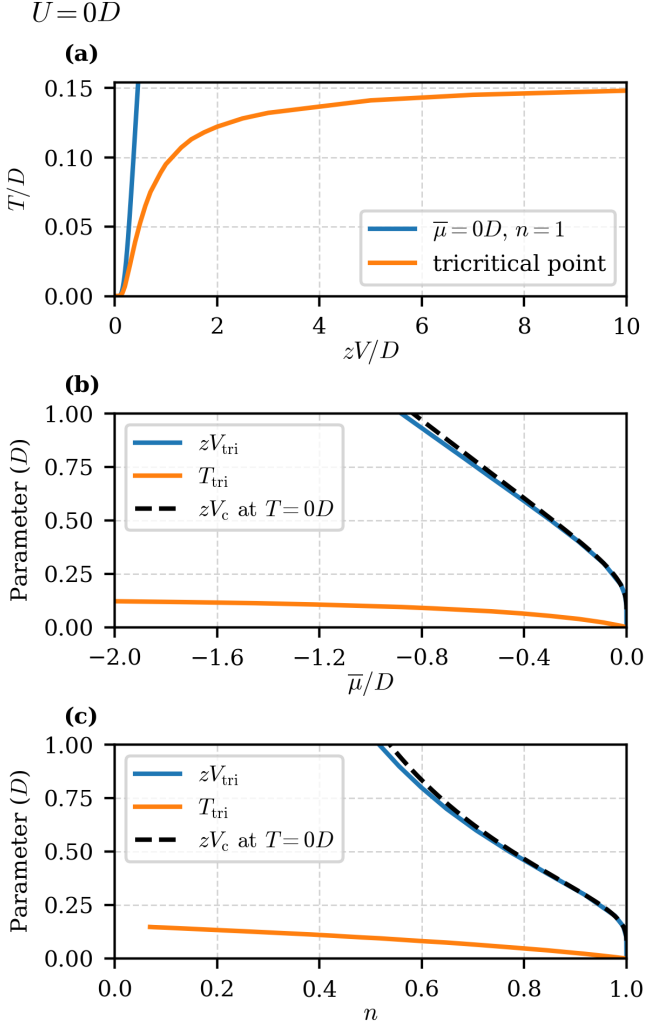
**(a)**



**(b)**



**(c)**



FIG. 5. Tendencies of the finite-temperature tricritical point for $U = 0D$: relation between the intersite interaction strength and temperature of the tricritical point, alongside with a point of the continuous CO-NO transition at $\bar{\mu} = 0D$ (eq. (31), Fig. 4a) (a); and dependencies of the intersite interaction strength and temperature of the tricritical point on the shifted chemical potential (b) and the electron density of the NO phase (c), alongside with a point of the discontinuous COI-NO transition at $T = 0D$ ($V_c$, Fig. 2a).

When both nonzero $U$ (Fig. 3a) and nonzero $T$ (Fig. 5a) act together, the discontinuous transition and phase-separated states disappear even faster.

The increase of $U$ reduces the temperatures in which the CO phase can occur. It follows from the fact that the maximum $T_c$ is at $\bar{\mu} = 0D$ and depends solely on the difference $(zV - \frac{U}{2})$, as discussed above. The short dashed lines in Fig. 4b show the evolution of the phase diagram as the $(zV - \frac{U}{2})$ stays constant while both $zV$ and $U$ increase. The discontinuous CO-NO transition quickly disappears, and the whole region of CO phases becomes elongated along the $\bar{\mu}$ axis.

A noticeable feature of the finite-temperature phase diagram is the reentrant behaviour of the CO phase: for a certain range of the chemical potentials, the CO phase is not stable at the ground state, but becomes stable as the temperature increases, before the increasing entropy contribution eventually destroys it. Such a reentrancy region becomes larger when $zV$ increases (see Fig. 4b). The competition between the electron itineracy ($t$-term) and localization due to the intersite repulsion ($V$-term) favors the NO phase at the ground state, but the increase of temperature changes the balance towards the CO phase.

It is clear from the color map plot of the parameter $c$ (eq. (19)) that the CO phase is rather insulating far from the CO-NO transition. Metallic properties is a necessary step towards the transition to the NO phase.

## VI. CONCLUSIONS AND FINAL REMARKS

The comprehensive analysis of the mean-field solution of the two-sublattice extended Hubbard model on the Bethe lattice is presented. We have filled the gap in literature to identify the correlation-induced effects and interpret the non-strongly-correlated phase, and presented the results that can be used in pedagogical purposes.

Comparing the results with DMFT results [48] a few conclusions can be made. Most obvious, strong enough local correlations cause the formation of a non-charge-ordered Mott insulator around the $\bar{\mu} = 0D$; and, for $U \gtrsim D$ and finite $zV$, the formation of a quarter-filled charge-ordered insulator on the border between NO and COM phases. Moreover, the strong-correlation effects remove the asymptotic behaviour of the COM and COI phases when approaching to the $\bar{\mu} = 0D$ and $zV = \frac{U}{2}$. The continuous COI-NO transition at $\bar{\mu} = 0D$ and $zV = \frac{U}{2}$ becomes discontinuous at around $zV = U$. The COM phase does not appear for $|\bar{\mu}| \lesssim \frac{U}{2}$ and the continuous COM-NO transition happens for smaller values of $zV$. Meanwhile, when the COM phase exists, the line of the COI-COM transition nicely reproduced by our mean-field results and less affected by the correlation effects.

Worth noting, that the neglected here magnetic order would be especially relevant for $zV < \frac{U}{2}$.

We also showed the importance of analytical simplifications in the considered model. For the ground state, the numerical integration around sophisticated points (the continuous phase-transition points, the $\bar{\mu} = 0D$ and $|\bar{\mu}| = zV + \frac{U}{2} + D$ points) leads to numerical inaccuracies that prevent from correct identification of the phase-transition lines. Moreover, the symmetry-broken phases require enormous number of iterations for the convergence close to the continuous transition to the non-charge-ordered phase, which can be avoided with analytical derivations. The mentioned problems appear when such analytical simplifications are not possible, and may be even harder to deal with when we have to sum over momentum vectors instead of the numerical integration. We expect that it is as well relevant for other self-

consistent methods (such as DMFT) when one considers any ordering phenomena. We thus expect, that even in the limit of the infinite coordination number (where the DMFT is precise), it can be hard to extract the quantitatively precise results from DMFT for the continuous symmetry-breaking transitions.

One should mention that, for $U = 0D$ the model (1) is equivalent to a spinless fermion model [34–44]. The structure of the diagram obtained in this regime is in agreement with the previous studies where the other shapes of the DOS were used (the qualitative differences for phase boundaries are very small) [35, 37–44]. Notice that for $U = 0D$, the COM phase is not present on the phase diagrams and is unstable for any $n$ ($\partial n/\partial \mu < 0$). However, the incommensurate orderings, which are not analyzed in this work, might also be possible with [44] and without (when $zV$ is not too large) a next-nearest-neighbor hopping [35, 38]. In the presence of the next-nearest-neighbor hopping, the COM can be stable at the ground state [42].

On an exemplary model studied in this work, i.e., the extended Hubbard model, we showed that, despite ignoring the correlation effects, the mean-field treatment of the model can provide significant insights into the problem (cf. [45, 48]). The Hartree-Fock MFA overestimates the stability of long-range orders and associated critical temperatures, but it can, nevertheless, give a qualitative description of the system in the ground state in certain interaction parameter ranges. Moreover, the non-correlated phases are found within the dynamical mean-field theory when the intersite interaction prevails over the on-site interaction [45, 48], while some other phases and phase transitions can have similar qualitative features as within the MFA. For comparison between results obtained with exact and mean-field treatment of on-site Hubbard interaction and for various strongly correlated models see e.g., the extended Falicov-Kimball model [61–63] and a model of superconductor with pair hopping [64, 65]).

[1] R. Micnas, J. Ranninger, and S. Robaszkiewicz, Superconductivity in narrow-band systems with local nonretarded attractive interactions, Rev. Mod. Phys. **62**, 113 (1990).

[2] T. Neupert, M. M. Denner, J.-X. Yin, R. Thomale, and M. Z. Hasan, Charge order and superconductivity in kagome materials, Nature Physics **18**, 220 (2022).

[3] M. Kang, S. Fang, J. Yoo, B. R. Ortiz, Y. M. Oey, J. Choi, S. H. Ryu, J. Kim, C. Jozwiak, A. Bostwick, E. Rotenberg, E. Kaxiras, J. G. Checkelsky, J.-H. P. Stephen D. Wilson, and R. Comin, Charge order landscape and competition with superconductivity in kagome metals, Nature Materials **22**, 186 (2023).

[4] E. Morosan, H. W. Zandbergen, B. Dennis, J. Bos, Y. Onose, T. Klimczuk, A. Ramirez, N. Ong, and R. J. Cava, Superconductivity in $Cu_xTiSe_2$, Nature Physics **2**, 544 (2006).

[5] A. M. Novello, B. Hildebrand, A. Scarfato, C. Didiot, G. Monney, A. Ubaldini, H. Berger, D. R. Bowler, P. Aebi, and C. Renner, Scanning tunneling microscopy of the charge density wave in $1T − TiSe_2$ in the presence of single atom defects, Phys. Rev. B **92**, 081101 (2015).

[6] K. Hiraki and K. Kanoda, Wigner crystal type of charge ordering in an organic conductor with a quarter-filled band: $(DI − DCNQI)_2Ag$, Phys. Rev. Lett. **80**, 4737 (1998).

[7] Y. Noda and M. Imada, Quantum phase transitions to charge-ordered and wigner-crystal states under the interplay of lattice commensurability and long-range coulomb interactions, Phys. Rev. Lett. **89**, 176803 (2002).

[8] A. Kumar, C. Lewandowski, and H. J. Changlani, Origin and stability of generalized wigner crystallinity in triangular moiré systems, npj Quantum Materials **10**, 95 (2025).

[9] Y. Kuramoto, Wigner crystal, electron chain, and charge density wave in strong magnetic fields, J. Phys. Soc. Jpn. **44**, 1572 (1978).

[10] M. Matty and E.-A. Kim, Melting of generalized wigner crystals in transition metal dichalcogenide heterobilayer Moiré systems, Nat. Commun. **13**, 7098 (2022).

[11] Y. Tan, P. K. H. Tsang, V. Dobrosavljević, and L. Rademaker, Doping a Wigner-Mott insulator: Exotic charge orders in transition metal dichalcogenide moiré heterobilayers, Phys. Rev. Research **5**, 043190 (2023).

[12] S. Robaszkiewicz, The charge-ordered state in an extended Hubbard model, Physica Status Solidi (b) **59**, K63 (1973).

[13] S. Robaszkiewicz, Electron-charge ordering and insulator-metal transition in an extended Hubbard model, Acta Phys. Polon. A **45**, 289 (1974).

[14] J. E. Hirsch, Charge-density-wave to spin-density-wave transition in the extended Hubbard model, Phys. Rev. Lett. **53**, 2327 (1984).

[15] J. E. Hirsch, Phase diagram of the one-dimensional molecular-crystal model with coulomb interactions: Half-filled-band sector, Phys. Rev. B **31**, 6022 (1985).

[16] H. Q. Lin and J. E. Hirsch, Condensation transition in the one-dimensional extended Hubbard model, Phys. Rev. B **33**, 8155 (1986).

[17] J. Hubbard, Electron correlations in narrow energy bands, Proceedings of the Royal Society of London. Series A. Mathematical and Physical Sciences **276**, 238 (1963).

[18] D. R. Penn, Stability theory of the magnetic phases for a simple model of the transition metals, Phys. Rev. **142**, 350 (1966).

[19] K. A. Chao, R. Micnas, and S. Robaszkiewicz, Charge-ordered ground state of a half-filled Hubbard model with strong intra-atomic attraction, Phys. Rev. B **20**, 4741

(1979).

[20] J. Spałek, A. Datta, and J. M. Honig, Discontinuous metal-insulator transitions and fermi-liquid behavior of correlated electrons, Phys. Rev. Lett. **59**, 728 (1987).

[21] R. Micnas, S. Robaszkiewicz, and K. Chao, Multicritical behavior of the extended Hubbard model in the zero-bandwidth limit, Phys. Rev. B **29**, 2784 (1984).

[22] C. Borgs, J. Jedrzejewski, and R. Koteckỳ, The staggered charge-order phase of the extended Hubbard model in the atomic limit, J. Phys. A: Math. Gen. **29**, 733 (1996).

[23] J. Fröhlich, L. Rey-Bellet, and D. Ueltschi, Quantum lattice models at intermediate temperature, Commun. Math. Phys. **224**, 33 (2001).

[24] F. Mancini and F. P. Mancini, One-dimensional extended Hubbard model in the atomic limit, Phys. Rev. E **77**, 061120 (2008).

[25] K. Kapcia, W. Kłobus, and S. Robaszkiewicz, Charge orderings and phase separations in the atomic limit of the extended Hubbard model with intersite density-density interactions, Acta Phys. Polon. A **118**, 350 (2010).

[26] K. Kapcia and S. Robaszkiewicz, The effects of the next-nearest-neighbour density–density interaction in the atomic limit of the extended Hubbard model, J. Phys.: Condens. Matter **23**, 105601 (2011).

[27] K. Kapcia and S. Robaszkiewicz, The effects of the next-nearest-neighbour density–density interaction in the atomic limit of the extended Hubbard model, J. Phys.: Condens. Matter **23**, 249802 (2011).

[28] K. Kapcia and S. Robaszkiewicz, Charge orderings and phase separations in the atomic limit of the extended Hubbard model with intersite density-density interactions, Acta Phys. Polon. A **121**, 1029 (2012).

[29] K. J. Kapcia and S. Robaszkiewicz, On the phase diagram of the extended Hubbard model with intersite densityâ€"density interactions in the atomic limit, Physica A **461**, 487 (2016).

[30] G. Pawłowski, Charge orderings in the atomic limit of the extended Hubbard model, Eur. Phys. J. B **53**, 471 (2006).

[31] G. Pawłowski and T. Kaźmierczak, Phase separation and critical phenomena in the charge ordered system, Solid State Commun. **145**, 109 (2008).

[32] G. Ganzenmüller and G. Pawłowski, Flat histogram monte carlo sampling for mechanical variables and conjugate thermodynamic fields with example applications to strongly correlated electronic systems, Phys. Rev. E **78**, 036703 (2008).

[33] A. Alekseev, A. Cichy, and K. J. Kapcia, Particle-hole asymmetry and pinball liquid in a triangular-lattice extended Hubbard model within the mean-field approximation, Phys. Rev. B **112**, 115155 (2025).

[34] R. Vlaming, G. S. Uhrig, and D. Vollhardt, Anomalous effects in interacting spinless fermion systems with local disorder, J. Phys.: Condens. Matter **4**, 7773 (1992).

[35] G. Uhrig and R. Vlaming, Inhibition of phase separation and appearance of new phases for interacting spinless fermions, Phys. Rev. Lett. **71**, 271 (1993).

[36] G. S. Uhrig and R. Vlaming, Interacting spinless fermions with disorder: the mott transition for infinite coordination number, J. Phys.: Condens. Matter **5**, 2561 (1993).

[37] R. Shankar, Renormalization-group approach to interacting fermions, Rev. Mod. Phys. **66**, 129 (1994).

[38] G. Uhrig and R. Vlaming, Zero and finite temperature phase diagram of the spinless fermion model in infinite

dimensions, Annalen der Physik **507**, 778 (1995).

[39] M. Y. Kagan and K. I. Kugel, Inhomogeneous charge distributions and phase separation in manganites, Physics-Uspekhi **44**, 553 (2001).

[40] Y. Zhang, M.-T. Tran, V. Yushankhai, and P. Thalmeier, Metal-insulator transition in the quarter-filled frustrated checkerboard lattice, Eur. Phys. J. B **44**, 265 (2005).

[41] P. Fulde, P. Thalmeier, and G. Zwicknagl, Strongly correlated electrons, in Solid State Phys., Vol. 60 (Elsevier, 2006) pp. 1–180.

[42] W. R. Czart, S. Robaszkiewicz, and B. Tobijaszewska, Charge ordering and phase separations in the spinless fermion model with repulsive intersite interaction, Acta Phys. Polon. A **114**, 129 (2008).

[43] W. R. Czart, P. R. Grzybowski, M. Nogala, and S. Robaszkiewicz, Effects of frustrating hopping on charge ordered states in itinerant fermion systems for arbitrary concentration in 2d lattice, Acta Phys. Polon. A **121**, 828 (2012).

[44] W. R. Czart, P. R. Grzybowski, M. Nogala, and S. Robaszkiewicz, Charge orderings and phase separations in itinerant fermion systems at half filling, Acta Phys. Polon. A **121**, 1042 (2012).

[45] A. Amaricci, A. Camjayi, K. Haule, G. Kotliar, D. Tanasković, and V. Dobrosavljević, Extended Hubbard model: Charge ordering and wigner-mott transition, Phys. Rev. B **82**, 155102 (2010).

[46] R. Pietig, R. Bulla, and S. Blawid, Reentrant charge order transition in the extended Hubbard model, Phys. Rev. Lett. **82**, 4046 (1999).

[47] N.-H. Tong, S.-Q. Shen, and R. Bulla, Charge ordering and phase separation in the infinite dimensional extended Hubbard model, Phys. Rev. B **70**, 085118 (2004).

[48] K. J. Kapcia, S. Robaszkiewicz, M. Capone, and A. Amaricci, Doping-driven metal-insulator transitions and charge orderings in the extended Hubbard model, Phys. Rev. B **95**, 125112 (2017).

[49] J. Merino, Nonlocal coulomb correlations in metals close to a charge order insulator transition, Phys. Rev. Lett. **99**, 036404 (2007).

[50] T. Ayral, P. Werner, and S. Biermann, Spectral properties of correlated materials: Local vertex and nonlocal two-particle correlations from combined gw and dynamical mean field theory, Phys. Rev. Lett. **109**, 226401 (2012).

[51] T. Ayral, S. Biermann, and P. Werner, Screening and nonlocal correlations in the extended Hubbard model from self-consistent combined gw and dynamical mean field theory, Phys. Rev. B **87**, 125149 (2013).

[52] L. Huang, T. Ayral, S. Biermann, and P. Werner, Extended dynamical mean-field study of the Hubbard model with long-range interactions, Phys. Rev. B **90**, 195114 (2014).

[53] H. Terletska, S. Iskakov, T. Maier, and E. Gull, Dynamical cluster approximation study of electron localization in the extended Hubbard model, Phys. Rev. B **104**, 085129 (2021).

[54] S. Iskakov, H. Terletska, and E. Gull, Single- and two-particle finite size effects in interacting lattice systems, Phys. Rev. B **106**, 235106 (2022).

[55] L. Philoxene, V. H. Dao, and R. Frésard, Charge collective modes in correlated electron systems: Plasmons beyond the random phase approximation, Phys. Rev. B **110**, 115143 (2024).

[56] S. Kundu and D. SĂ©nĂ©chal, CDMFT+HFD: An extension of dynamical mean field theory for nonlocal interactions applied to the single band extended Hubbard model, SciPost Phys. Core **7**, 033 (2024).

[57] A. Georges, G. Kotliar, W. Krauth, and M. J. Rozenberg, Dynamical mean-field theory of strongly correlated fermion systems and the limit of infinite dimensions, Rev. Mod. Phys. **68**, 13 (1996).

[58] E. Arrigoni and G. C. Strinati, Doping-induced incommensurate antiferromagnetism in a mott-Hubbard insulator, Phys. Rev. B **44**, 7455 (1991).

[59] M. Bąk, Mixed phase and bound states in the phase diagram of the extended Hubbard model, Acta Phys. Polon. A **106**, 637 (2004).

[60] W. R. Czart, P. R. Grzybowski, and S. Robaszkiewicz, Charge ordering and phase separations in the molecular crystal model, Acta Phys. Polon. A **118**, 369 (2010).

[61] R. Lemański, K. J. Kapcia, and S. Robaszkiewicz, Extended Falicov-Kimball model: Exact solution for the ground state, Phys. Rev. B **96**, 205102 (2017).

[62] K. J. Kapcia, R. Lemański, and S. Robaszkiewicz, Extended falicov-kimball model: Exact solution for finite temperatures, Phys. Rev. B **99**, 245143 (2019).

[63] K. J. Kapcia, R. LemaĹ„ski, and M. J. Zygmunt, Extended falicov–kimball model: Hartree–fock vs dmft approach, J. Phys.: Condens. Matter **33**, 065602 (2020).

[64] K. J. Kapcia and W. R. Czart, Ground state phase diagram of the extended Hubbard model with pair-hopping interaction in the limit of very narrow bandwidth, Acta Phys. Polon. A **130**, 617 (2016).

[65] K. J. Kapcia and W. R. Czart, Phase separations in the narrow-bandwidth limit of the Penson-Kolb-Hubbard model at zero temperature, Acta Phys. Polon. A **133**, 401 (2018).